(1)

SRI International

AD-A279 932

Quarterly Technical Report 9 • 27 May 1994

FIELD-EMITTER ARRAYS FOR RF VACUUM MICROELECTRONICS

C.A. Spindt, Program Director
Physical Electronics Laboratory

SRI Project 2743

Prepared for:

Advanced Research Projects Agency
Defense Sciences Office
Virginia Square Plaza
3701 North Fairfax Drive
Arlington, VA 22203-1714

Attn: Dr. Bertram H. Hui

DTIC
ELECTE
JUN 06 1994
S B D

QUALITY INSPECTED 3

ARPA Order No. 8162

Contract MDA972-91-C-0029

Covering the Period 1 October through 31 December 1993

The views and conclusions contained in this document are those of the authors and should not be interpreted as representing the official policies, either expressed or implied, of the Advanced Research Projects Agency or the U.S. Government.

APPROVED FOR PUBLIC RELEASE
DISTRIBUTION UNLIMITED

94-16625

94 6 3 070

333 Ravenswood Avenue • Menlo Park, CA 94025-3493 • (415) 326-6200 • FAX (415) 326-5512 • Telex: 334486

FIELD-EMITTER ARRAYS FOR RF VACUUM MICROELECTRONICS

C.A. Spindt, Program Director
Physical Electronics Laboratory

SRI Project 2743

Prepared for:

Advanced Research Projects Agency
Defense Sciences Office
Virginia Square Plaza
3701 North Fairfax Drive
Arlington, VA 22203-1714

Attn: Dr. Bertram H. Hui

ARPA Order No. 8162

Contract MDA972-91-C-0029

Covering the Period 1 October through 31 December 1993

The views and conclusions contained in this document are those of the authors and should not be interpreted as representing the official policies, either expressed or implied, of the Advanced Research Projects Agency or the U.S. Government.

APPROVED FOR PUBLIC RELEASE
DISTRIBUTION UNLIMITED

Approved:

Eric Pearson, Director
Physical Electronics Laboratory

Donald L. Nielson, Vice President
Computing and Engineering Sciences Division

SRI International 333 Ravenswood Avenue • Menlo Park, CA 94025-3493 • (415) 326-6200 • FAX: (415) 326-5512 • Telex: 334486

REPORT DOCUMENTATION PAGE

Form Approved
OMB No. 0704-0188

Public reporting burden for this collection of information is estimated to average 1 hour per response, including the time for reviewing instructions, searching existing data sources, gathering and maintaining the data needed, and completing and reviewing the collection of information. Send comments regarding this burden estimate or any other aspect of this collection of information, including suggestions for reducing this burden, to Washington Headquarters Services, Directorate for Information Operations and Reports, 1215 Jefferson Davis Highway, Suite 1204, Arlington, VA 22202-4302, and to the Office of Management and Budget, Paperwork Reduction Project (0704-0188), Washington, DC 20503.

1. AGENCY USE ONLY (Leave Blank)	2. REPORT DATE	3. REPORT TYPE AND DATES COVERED
	27 May 1994	Quarterly Technical 9 (1 Sept. to 31 Dec. 1993)

4. TITLE AND SUBTITLE

Field-Emitter Arrays for RF Vacuum Microelectronics

5. FUNDING NUMBERS

6. AUTHORS

C.A. Spindt

7. PERFORMING ORGANIZATION NAME(S) AND ADDRESS(ES)

SRI International
333 Ravenswood Avenue
Menlo Park, CA 94025-3493

8. PERFORMING ORGANIZATION REPORT NUMBER

9. SPONSORING/MONITORING AGENCY NAME(S) AND ADDRESS(ES

Advanced Research Projects Agency/Defense Sciences Office
Virginia Square Plaza
3701 North Fairfax Drive
Arlington, Virginia 22203-1714

10. SPONSORING/MONITORING AGENCY REPORT NUMBER

11. SUPPLEMENTARY NOTES

12a. DISTRIBUTION/AVAILABILITY STATEMENT

Approved for public release; distribution unlimited

12b. DISTRIBUTION CODE

13. ABSTRACT *(Maximum 200 words)*

SRI International has completed the ninth quarter of a program to develop field-emitter arrays for vacuum microelectronics. We have met the first-phase program goals of 5 mA total emission, with a current density of 5 A/cm^2 for at least 2 hours and demonstrated modulation of the emission current at a frequency of 1 GHz.

An evaluation was made of deposition processes and cone materials that could lead to improved (tall and sharp) cone geometries for low-capacitance cathode fabrication. Principal efforts involved investigation of the limited emission of high-frequency cathode samples, continued stability tests on high-frequency cathodes to determine the effectiveness of processes designed to avoid contamination, and capacitance measurements on cathode samples incorporating an electrostatic shield designed to prevent fringing fields from the base electrode from influencing the trajectories of emitted electrons.

14. SUBJECT TERMS

Field-emitter array, vacuum microelectronics, low-capacitance cathode

15. NUMBER OF PAGES

44

16. PRICE CODE

17. SECURITY CLASSIFICATION OF REPORT	18. SECURITY CLASSIFICATION OF THIS PAGE	19. SECURITY CLASSIFICATION OF ABSTRACT	20. LIMITATION OF ABSTRACT
Unclassified	Unclassified	Unclassified	Unlimited

EXECUTIVE SUMMARY

SRI International has completed the ninth quarter of Phase I of a research and development program on the SRI Spindt-type field-emitter-array cathode with a view toward eventual applications in microwave amplifiers. We have met the first-phase goals of 5 mA total emission, with a current density of 5 A/cm^2 for at least 2 hours and demonstrated modulation of the emission current at a frequency of 1 GHz. Our approach has been to identify methods of adapting and modifying the basic cathode structure of microwave operation and to experimentally investigate means of implementing those methods.

During the quarter we have accomplished the following, as documented in detail in this technical report:

- Continued research on basic cathode technology as defined by the goals of the ARPA program and related NRL project (Section 1)
- Evaluated deposition processes and cone materials that could lead to improved (tall and sharp) cone geometries for low-capacitance cathode fabrication (Section 2)
- Investigated the limited emission of high-frequency cathode samples delivered to NRL, continued stability tests on high-frequency cathodes to determine the effectiveness of processes designed to avoid contamination, and performed capacitance measurements on cathode samples incorporating an electrostatic shield designed to prevent fringing fields from the base electrode from influencing the trajectories of emitted electrons (Section 3)
- Planned activities for the period of 1 January through 31 March 1994 (Section 5)

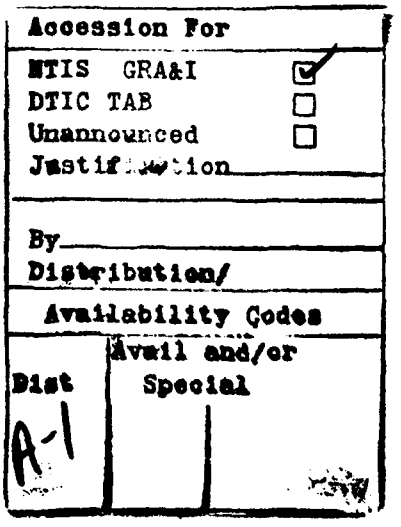

CONTENTS

1. INTRODUCTION 1

2. LOW-CAPACITANCE CATHODE FABRICATION 2

3. EMISSION TESTS 5

   3.1 Cathodes Shipped to NRL 6

   3.2 Contamination Tests 6

   3.3 Effects of the Electrostatic Shield 12

4. HIGH-FREQUENCY MEASUREMENTS 12

5. PROCESSING TO IMPROVE YIELD AND RELIABILITY 12

6. WORK PLANNED 13

APPENDIX

Glow Discharge Processing to Enhance Field-Emitter Array Performance A-1

ILLUSTRATIONS

1. Scanning electron micrographs of two recent low-capacitance cathodes showing varying, and less than optimum, cone shapes 3
2. Point at which cracks tend to initiate in the composite closure film 5
3. Scanning electron micrographs of gate apertures from opposite sides of a low-frequency cathode substrate 7
4. Current/voltage characteristics for three low-capacitance cathodes and three standard 10,000-tip cathodes on silicon operated at the same time in the same test chamber for comparison 8
5. Fowler/Nordheim data for three high-frequency cathodes and one "standard" 10,000-tip cathode 10
6. Capacitances measured at NRL 11

1. INTRODUCTION

SRI International is participating in an effort of the Advanced Research Projects Agency (ARPA) and the Naval Research Laboratory (NRL) to perform research and development on the SRI Spindt-type field-emitter-array cathode with a view toward eventual applications in microwave amplifiers. The current ARPA program is the vehicle for advancing the basic cathode technology for microwave applications (e.g., reducing intrinsic capacitance and driving voltage requirements), and continues the original program plan to establish the characteristics of the cathode in its preprogram state of development, identify methods of adapting and modifying the structure for microwave operation, and experimentally investigate means of implementing those methods. For the NRL program, which began earlier than the ARPA project, SRI has shifted emphasis to the support of NRL's in-house vacuum microelectronics program by providing NRL with state-of-the-art Spindt-type cathodes and consultation on setting up and using cathodes. We have met the first-phase program goals of 5 mA total emission, with a current density of 5 A/cm^2 for at least 2 hours and demonstrated modulation of the emission current at a frequency of 1 GHz.

At the beginning of the program, two areas of development required immediate attention. The first was a materials and processing issue related to providing and maintaining a suitable vacuum environment for the cathodes. The second related to the cathode's inherent high capacitance and means for reducing that capacitance to a level that is consistent with the microwave applications envisioned for the cathode.

Our approach has been to research these two issues in parallel, using an easy-to-build, low-frequency-triode configuration fabricated on a TO-5 header as a test vehicle for materials and processing studies, and at the same time designing and researching fabrication techniques for building high-frequency-cathode structures on dielectric substrates (e.g., quartz or glass). Specific tasks that are being addressed on these related programs are

1. Fabrication of a supply of state-of-the-art cathodes for use in establishing cathode characteristics, and for developing structures, circuits, and procedures for testing the cathodes as triodes
2. Development of a close-spaced anode test configuration that can be used to investigate triode characteristics at low frequency (kHz to MHz) in order to study the known problems with cathode survival under close-spaced anode conditions
3. Development of a circuit for driving the cathodes and demonstrating gain, frequency response, and peak emission levels
4. Studies of advanced cathode structures (geometry, fabrication technology, and processing) for high-frequency operation

5. Investigations (with NRL) of cathode mounting and connecting procedures using practices that are consistent with the microwave goals of the effort

6. Consultations with the NRL staff on the experimental results and applications of the cathode technology

2. LOW-CAPACITANCE CATHODE FABRICATION

As described in the previous quarterly report, recent cone formation runs have been producing relatively inconsistent results and cones, shown in the scanning electron micrographs (SEMs) of Figure 1, that are not of our preferred geometry (tall and sharp). These variations were first noticed during the time when the more important task of solving the contamination problem dominated our efforts. Now that the contamination is being controlled, we are addressing the issue of inconsistent hole/cone geometry.

Cones are now formed by a well-known vacuum-deposition process that is very simple in principle. The top of a micrometer-size cavity (hole) is closed by rotating the cavity while vacuum depositing material onto its top inner edge from an evaporation source positioned to deposit this material at a shallow angle relative to the surface in which the cavity is formed. While the cavity is closing, the cone is formed within it by deposition of material from a second evaporator positioned normal to the surface so that it can deposit material on the bottom of the cavity. Because of the shallow-angle source deposition, this deposited material in the cavity is formed into a cone by the shadow-masking effect of the top inner edge of the cavity as it closes. The cone can be formed into a very sharp (~ 250 Å radius) tip if the process is done properly.

However, implementation of the process can be very demanding because several issues must be dealt with:

1. The uniformity of the holes in the gate film must be very good.

2. The cone will be too short if the hole is closed too rapidly.

3. The cone will be too tall if the hole is closed too slowly, and it will be blunt if the hole does not close completely.

4. If the ratio of deposited hole-closure material to cone is below a certain limit, the deposited composite film breaks up and ruins the sample.

5. If the ratio of deposited hole-closure material to cone is above a certain limit, the deposited composite film is very difficult or impossible to etch off of the substrate.

6. If the closure film is deposited at too shallow an angle, the cone formation material forms a "hood" over the hole that is difficult or impossible to remove.

7. If the closure film is deposited at too steep an angle, the cone will be too dull.

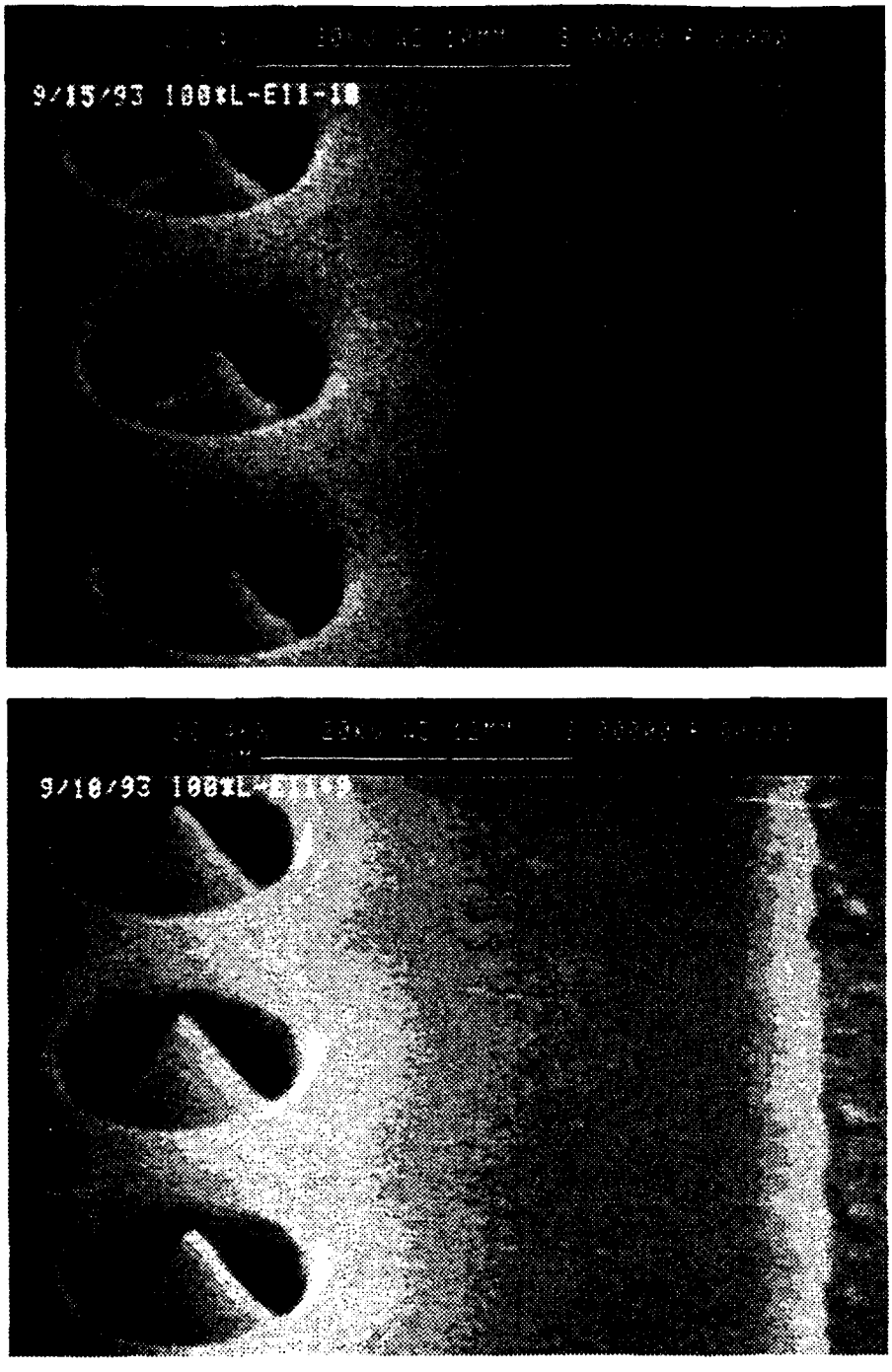

Figure 1. Scanning electron micrographs of two recent low-capacitance cathodes showing varying, and less than optimum, cone shapes

8. The optimum closure film deposition angle depends on the hole diameter and the gate film thickness, and therefore may have to be changed for any given sample.

9. The temperature of the substrate must be within certain limits or the cone will not stick, the film may crack, of the closure film may be very difficult to etch.

To achieve a perfect cone geometry, these and other parameters must be controlled, and some of them are contradictory.

The nature of the process makes it desirable to deposit a large amount of cone-forming material onto the substrate relative to the closure material, so as to produce a tall, sharp cone. However, this is always done at the risk of breaking up the sample because of the excessive stress buildup in the deposited film.

The cone material is always metallic, and deposits with tensile stresses that can be large enough to pull underlying layers away from, or even fracture, the substrate. The chosen closure film is a material that deposits with compressive stress to help compensate for the tensile stresses of the metal film, so that thicker layers can be achieved in order to form taller, sharper cones. Historically, aluminum oxide has been used as the closure film, and molybdenum has been the cone-formation material. We have learned now to control the deposition of these materials reasonably well for our "standard" cathodes formed on silicon substrates. However, the low-capacitance configuration is formed on glass so that the base electrode can be patterned into a microstrip line. This requires that an oxide be deposited over the base and a gate layer over the oxide. The resulting structure has a "step" at the edge of the patterned base electrode, over which the composite closure and cone material film is deposited. As mentioned above, the composite film has built-in residual stresses, and any discontinuity in the surface is a "stress riser." Sharp edges are bad, and sharp corners are especially bad.

Figure 2 is a plan view of a low-capacitance cathode. The base electrode is etched with standard photolithography, which must be very precisely done because of the tolerances involved in fabricating a 4-μm-wide, 1.25-mm-long overlap with the gate electrode having a row of 1-μm-diameter holes centered along its entire length. Because of the precision of the patterning, the edge of the base film and the corners are sharp and behave as stress risers. In hindsight, it might be better to have the corners of the base rounded to reduce stress, but the sharp step along the edge is unavoidable. Other solutions are to planarize the oxide layer prior to the gate film deposition, with smaller holes so that the required thickness—and therefore the total stress in the composite layer—is reduced, or to use alternative cone materials that have less inherent stress than the molybdenum.

Planarization can be done with a planarizing resist layer and reactive-ion etching or mechanical polishing after oxide deposition, followed by a second oxide deposition as necessary to produce the desired final oxide thickness. Alternative cone materials have some appeal in that no additional process steps would be required. In addition, the development of other cone materials may also lead to improved cone geometries because different materials naturally form taller or shorter cones, and it may also be possible to find a material with an improved work function with respect to molybdenum. Some preliminary investigations have shown that many materials—such as CR_xSi_y, Si, Nb, Cu, Th, Ni, and their combinations—are promising. The

difficulty lies in finding combinations that are compatible with the chemistry involved in the overall process. Then, the question of performance as a field emitter must also be addressed.

Some preliminary work with Cr_xSi_y has produced very nice looking structures, but in emission tests the Cr_xSi_y cathodes did not perform as well as cathodes fabricated with molybdenum tips. The overcoating of a material that forms nicely shaped tips with a material that produces a preferred field-emission surface may also be an option.

3. EMISSION TESTS

Several high-frequency cathode samples were shipped to NRL for in-house testing, and these efforts met with limited success. In work with the sulfur contamination problem studied earlier, we continued with tests to determine the stability of three high-frequency cathodes. We also continued work on the effects of electrostatic shielding.

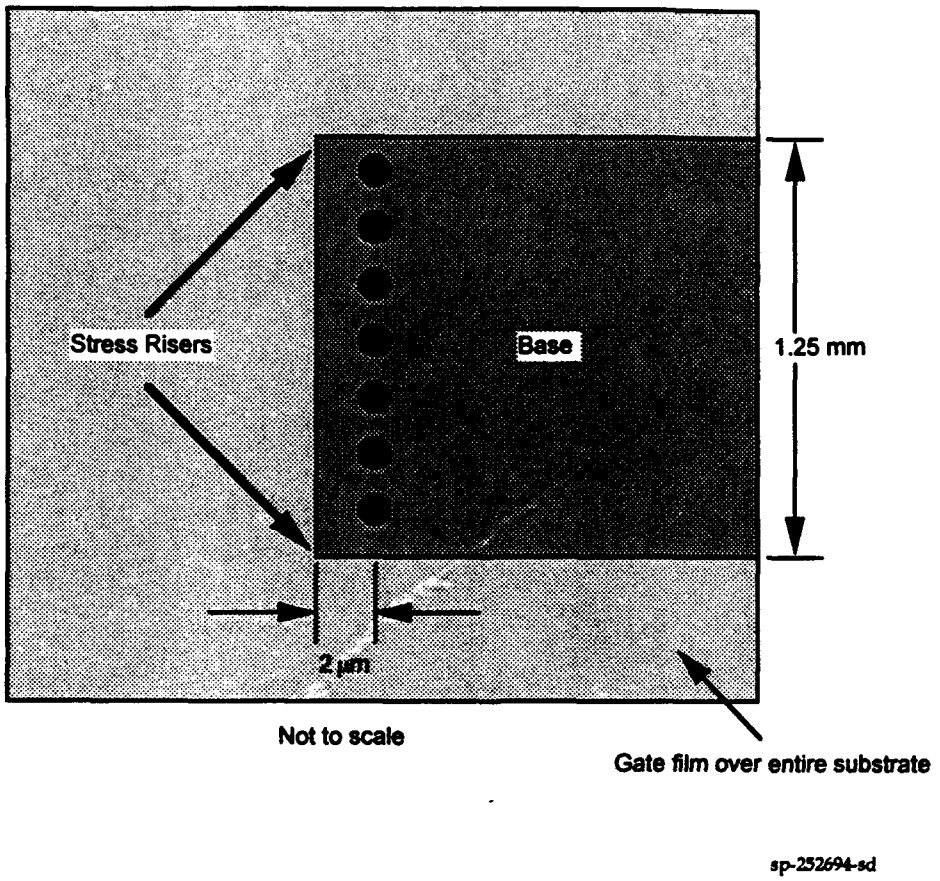

Figure 2. Point at which cracks tend to initiate in the composite closure film

3.1 CATHODES SHIPPED TO NRL

High-frequency cathode samples were shipped to NRL for in-house testing. Emission was obtained, but for the most part it was insufficient to permit high-frequency experiments, even with cathodes from batches that produced good results at SRI. Some of the cathodes examined at NRL showed mechanical damage that most likely occurred during the handling associated with shipping, while others were surprisingly different from what had been seen at SRI during SEM examinations of what were assumed to be representative samples from the same substrate. Normally, only a few representative samples from each substrate are examined in the SEM, because it is time-consuming and expensive (each substrate has 24 cathodes on it), and tends to leave detrimental contaminants (polymerized hydrocarbon layers) on the surfaces. It was thought that the holes on each substrate were essentially the same, and they appeared to be the same in the optical microscope, which does not have the resolution required to make accurate measurements of the hole diameters. However, it has turned out that while the hole diameters are almost always the same on each cathode, they are not the same from cathode to cathode over the same substrate. Figure 3 is an example showing 1.46-μm-diameter gate apertures for cathodes on one side of the substrate and 1.13-μm-diameter apertures in cathodes on the opposite side. We were surprised by this, because the lithography is done with a state-of-the-art stepper by a local semiconductor foundry that routinely meets stringent specifications.

In the future we will make more careful examination of cathodes sent to NRL to be certain that SRI and NRL test identical cathodes.

3.2 CONTAMINATION TESTS

During the past two reporting periods, a sulfur cathode-contamination problem due to reactive ion etching with SF_6 was identified, and a tentative solution to the problem by using CF_4 reactive ion etch as a final touch-up of the gate and base-shield electrodes was proposed. Results of an ongoing test with three cathodes to determine the stability of high-frequency cathodes were also reported.

During this period, the emission level of the three high-frequency cathodes was increased from 100 μA to 600 μA while being monitored for signs of instability. At the 400-μA level, two of the cathodes exhibited some transient erratic gate current in the 5-μA range, and one (103L-E11+5B) required a 10-V increase in drive voltage to maintain 400 μA. The other (102L-E11+5i) did not require a perceptible increase in voltage. At the 600-μA level, cathode 103L-E11+5B was clearly damaged because a significant increase in voltage was required to maintain emission. Oscillographs of the current/voltage characteristics were taken of the three high-frequency cathodes and the three standard 10,000-tip cathodes used as controls in the experiment. The test was then terminated so that the cathodes could be examined. The oscillographs shown in Figure 4 indicate that the three 10,000-tip control cathodes (52i-344-4C, 52i-344-4D, and 52i-344-4F) were performing normally at 1-mA peak emission, each with no gate current at the time of shutdown.

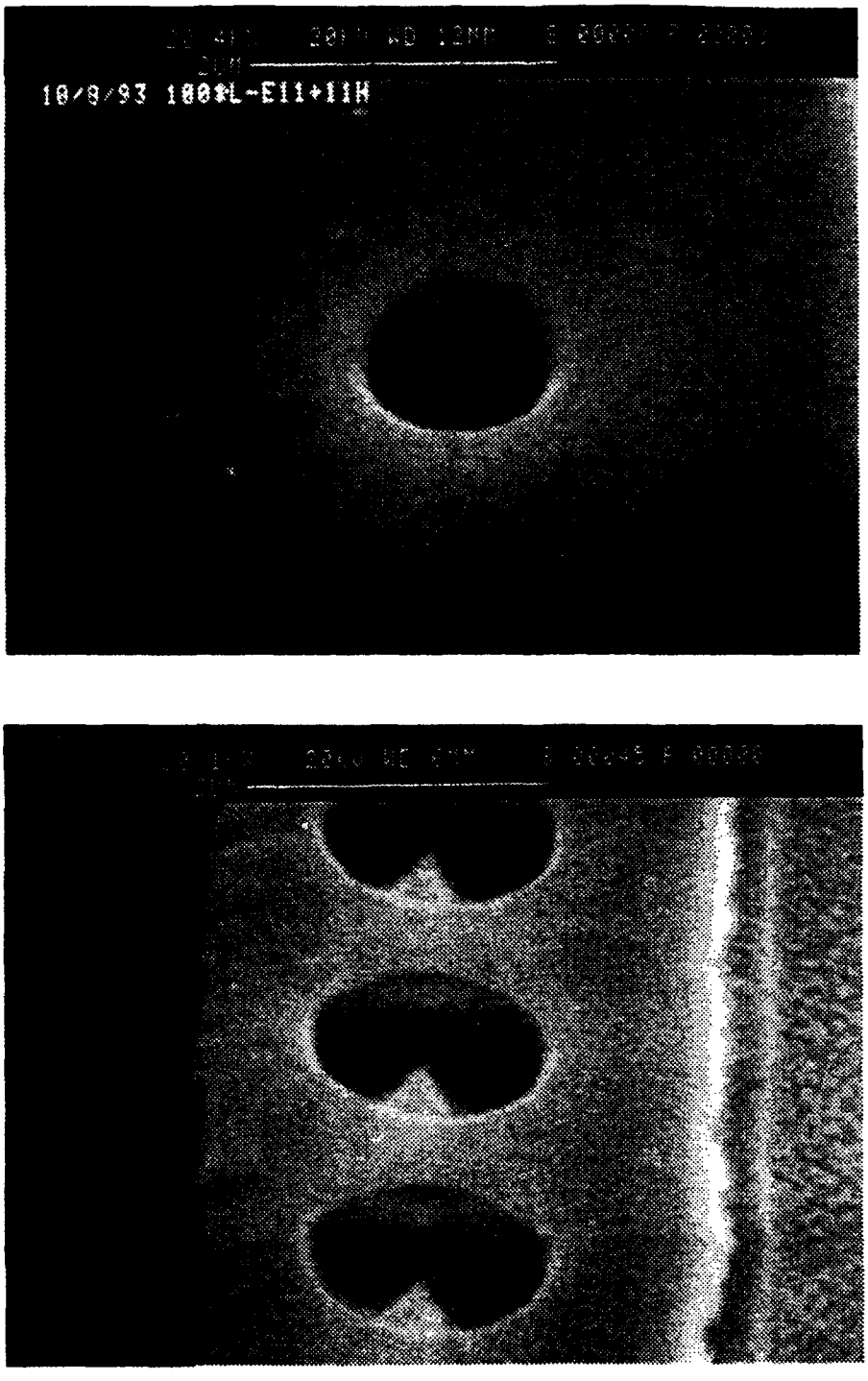

Figure 3. Scanning electron micrographs of gate apertures from opposite sides of a low-frequency cathode substrate (24 cathodes per substrate)

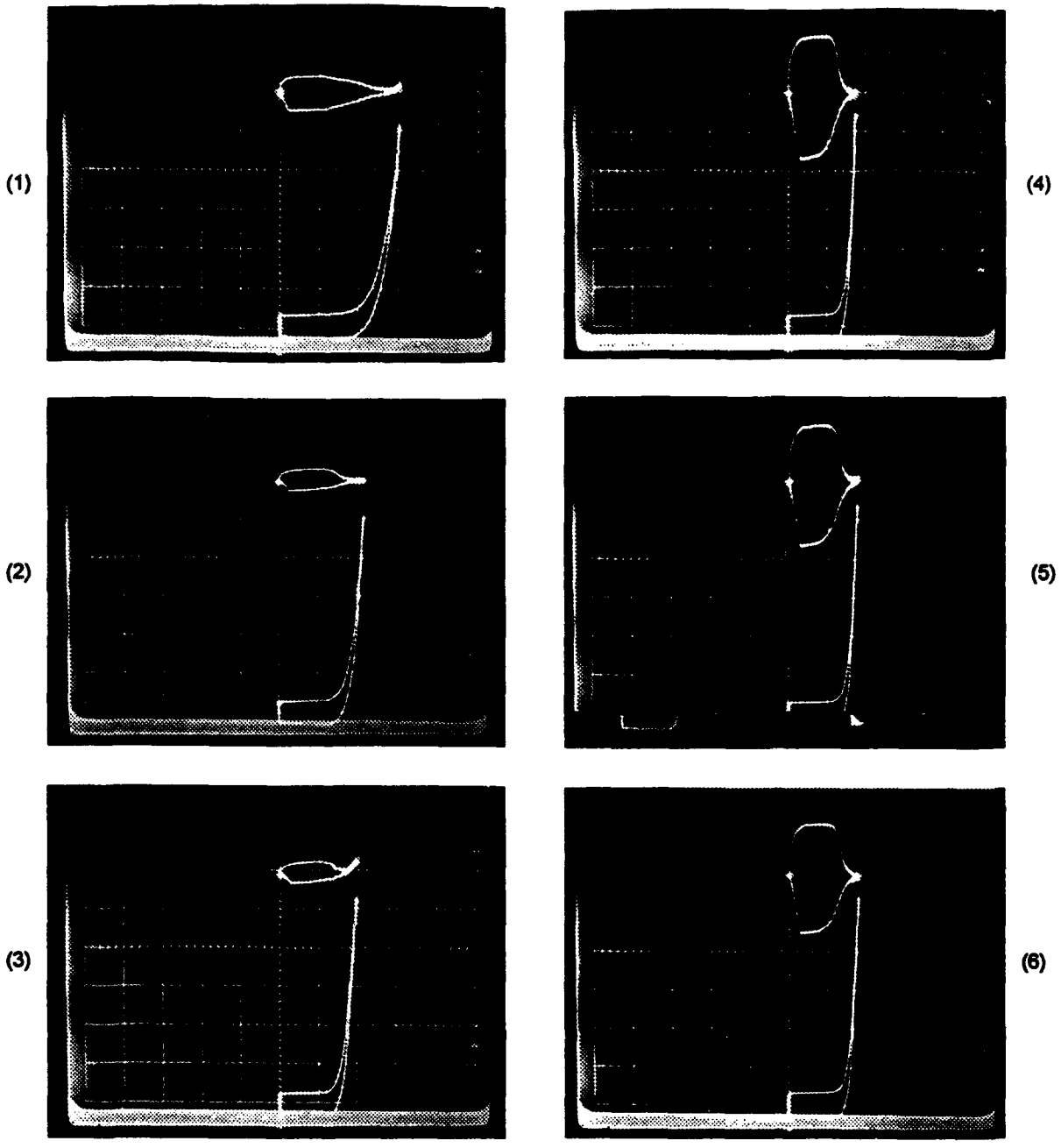

Horizontal: 50 V/Major Division
Vertical: 20 μA/Major Division

(1) Low-capacitance cathode 103L-E11+5B (250 tips)
(2) Low-capacitance cathode 102L-E11+5D (625 tips)
(3) Low-capacitance cathode 102L-E11+5i (625 tips)
(4) Standard cathode 52i-344-4C (10,000 tips)
(5) Standard cathode 52i-344-4D (10,000 tips)
(6) Standard cathode 52i-344-4F (10,000 tips)

Figure 4. Current/voltage characteristics for three low-capacitance cathodes and three standard 10,000-tip cathodes on silicon operated at the same time in the same test chamber for comparison

Figure 5 is a Fowler-Nordheim (F/N) plot of emission data taken at shutdown. (The control cathodes are plotted as one because they were so close together that they were indistinguishable in the F/N plot.) Because the high-frequency cathodes were all made on the same substrate at the same time, it was expected that the slopes of the F/N plots would be the same and the plots would be displaced only in proportion to the number of tips in each cathode. Figure 6 shows that this is indeed the case. All three plots are essentially parallel within the limits of experimental error and the best fit of the data. The "standard" cathodes, of course, were fabricated at a different time on a different substrate, and as a group have nearly identical plots, but could reasonably have a different slope than the high-frequency cathodes.

The cathodes were inspected optically after removal from the test chamber. The high-frequency cathodes were of two kinds; cathode #1 had 250 emitters on 5-μm centers (103L-E11+5B), and cathodes #2 and #3 each had 625 emitters on 2-μm centers (102L-E11+5D and 102L-E11+5i, respectively). The standard control cathodes—#4, #5, and #6—were all 10,000-tip arrays on 8-μm centers. All six cathodes had approximately the same gate aperture diameters of about 1 μm.

The results of the optical inspection showed that cathode #1 had roughly half of its emitter tips blown away, cathode #2 was *totally undamaged*, and cathode #3 had nine tips blown away. With the gate apertures shown in Figure 3, it is surprising that cathode #1 was working as well as it was. It is also interesting that there is such a difference in the performance of cathodes from the same substrate. This is a clear demonstration of the need for more processing studies to determine what is causing these differences and to find ways to improve yield and reliability so that more cathodes behave like cathode #2.

The 10,000-tip control cathodes had very few emitter tips blown away and in such a mild fashion that it was difficult to spot them. Cathode #4 had two damaged tips, cathode #5 had six damaged tips, and cathode #6 had three damaged tips.

The large number of tips lost on cathode #1 probably explains the big difference in the level of emission between cathode #1 and cathodes #2 and #3. The difference between cathodes #2 and #3 is well within the 10% accuracy of the voltage-sensing resistors in the drive circuits used. For example, 100 μA emission was produced at 108 V and 100 V for cathodes #2 and #3, respectively. If the 108 V is decreased by 5% and 100 V is increased by 5%, they essentially overlap.

The conclusions that we draw from these results are that the contamination problem has been identified and a method for removing it has been developed. The mixed results of the emission tests show that the process is not yet perfect, but it is possible to fabricate and operate the high-frequency cathodes without failures because it has been done. It is now a question of working on the details of the processing to improve yield and reliability.

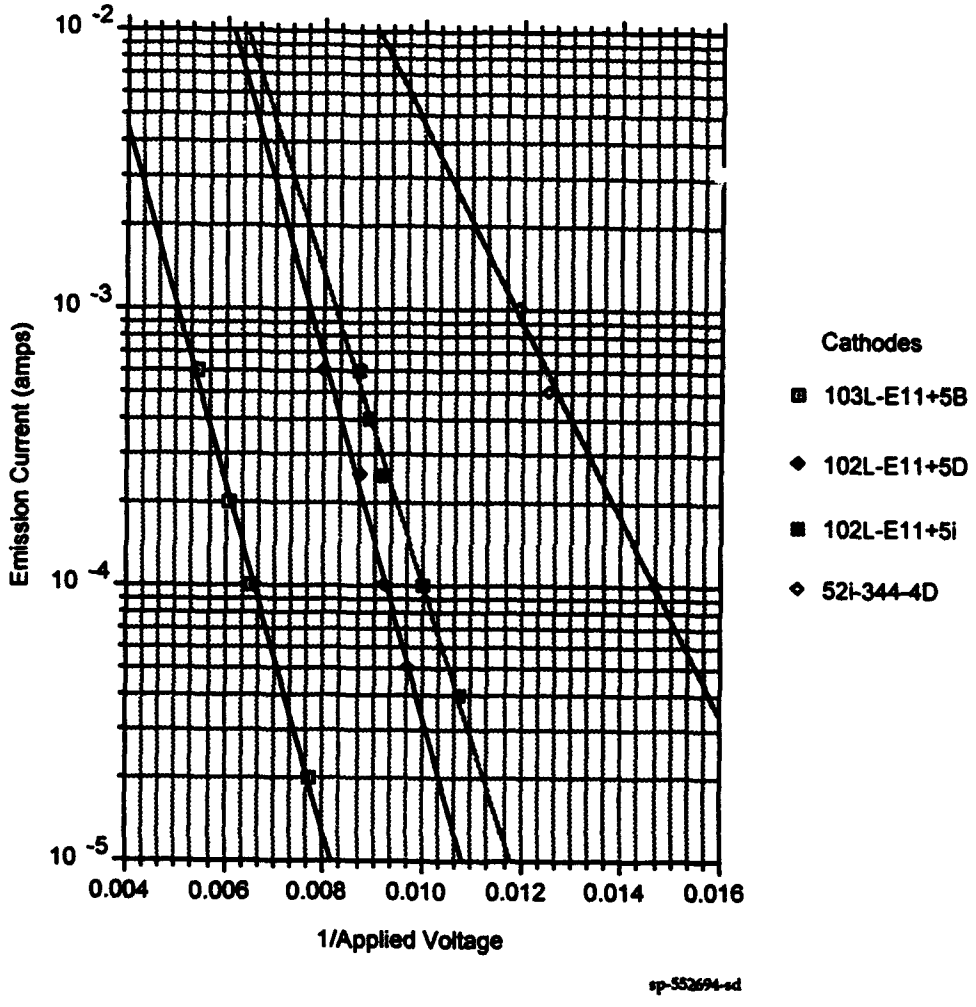

Figure 5. Fowler/Nordheim data for three high-frequency cathodes (103L = 250 tips, 102L = 625 tips) and one "standard" 10,000-tip cathode (52i)

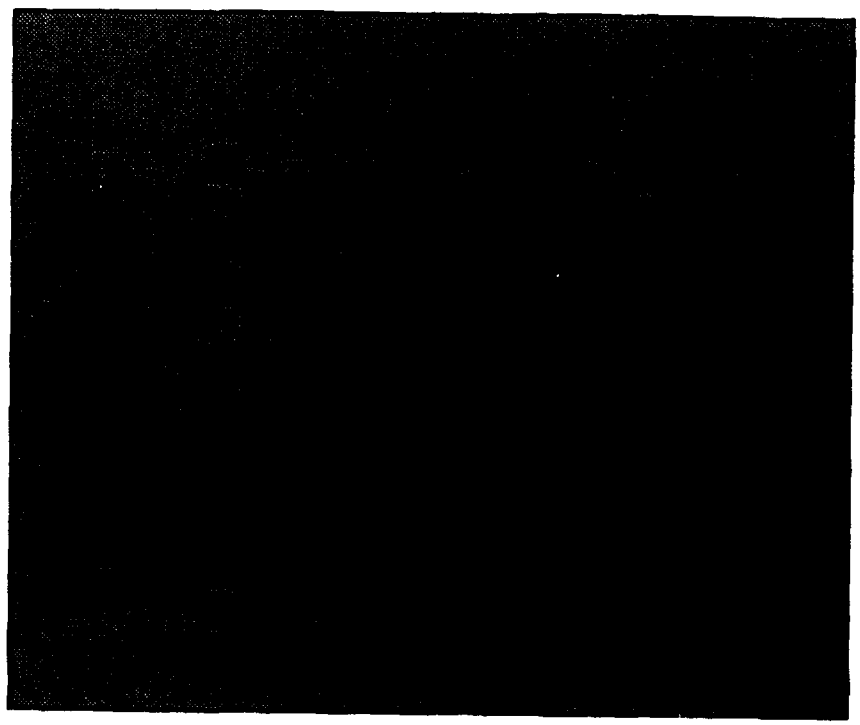

sp-652594-ad

Cgb = C3 + C1xC2/(C1+C2) = 0.60 pF

Ceb = C2 + C1xC3/(C1+C3) = 5.23 pF

Ceg = C1 + C2xC3/(C2+C3) = 0.56 pF

Cgb, Ceb, and Ceg were measured at NRL, and C1, C2, and C3 calculated as:

C1 = 0.16 pF

C2 = 5.11 pF

C3 = 0.44 pF

Figure 6. Capacitances measured at NRL

3.3 EFFECTS OF THE ELECTROSTATIC SHIELD

An electrostatic shield was designed to prevent fringing fields from the base electrode from influencing the trajectories of the emitted electrons. The details of the shield were described in the previous quarterly report. Careful capacitance measurements were made at NRL on cathode samples supplied by SRI to determine the shield's effects on gate capacitance. Figure 6 is a schematic diagram of the shield with the measured capacitances and the calculated capacitances based on the measurements. The results show that the shield added about 0.16 pF to the capacitance of the gate, for a total measured capacitance of 0.6 pF. This is in very good agreement with the expected gate capacitance extrapolated from measurements, made at SRI at the beginning of the program, on much larger electrode areas, using the same materials. Those results indicated that the capacitance for the high-frequency-cathode design should be in the 0.1- to 1.0-pF range, depending on the details of the hole diameters, cone geometries, oxide thickness, amount of oxide etch undercut (amount of oxide removed and replaced by vacuum), and width of the base and gate overlap area. (The overlap-area length is constant in the high-frequency configuration, and is determined by the substrate material and substrate thickness to match a 50-ohm microstrip line.)

4. HIGH-FREQUENCY MEASUREMENTS

No high-frequency measurements were made during this period.

5. PROCESSING TO IMPROVE YIELD AND RELIABILITY

Plasma cleaning processes are continuing in the emission microscope apparatus. The results have been very interesting and encouraging, and were submitted for publication to the *Journal of Applied Physics*. A preprint of the paper is attached as an appendix.

6. WORK PLANNED

Cathode fabrication and emission measurements will continue to evaluate the effect of processing steps designed to improve yield and reliability. Tests with *in situ* processing will also be continued to determine methods of improving emission uniformity, reducing operating voltage requirements, and improving yield.

Appendix

GLOW DISCHARGE PROCESSING TO ENHANCE FIELD-EMITTER ARRAY PERFORMANCE

Glow discharge processing to enhance field-emitter array performance

P.R. Schwoebel [Telephone: (415) 859-4845, FAX: (415) 859-3090] and

C.A. Spindt [Telephone: (415) 859-2993, FAX: (415) 859-3090]

SRI International, Menlo Park, California 94025

(Received

ABSTRACT

Changes in the electron-emission spatial distribution and I-V characteristics of microfabricated field emitters following inert gas ion bombardment have been investigated. The combination of glow discharge treatments in hydrogen and neon result in contaminant removal and mild emitter tip sputtering, thereby leading to significant improvements in the uniformity of the electron emission from individual tips and between tips in the arrays. The majority of the enhancement in the uniformity of the electron emission appears to be due to a net smoothing of the emitter tip surfaces through the removal of field-enhancing protuberances by the inert gas ion bombardment.

PACS numbers: 79.70.+q, 79.20.Nc, 81.60.Bn

I. INTRODUCTION

Microfabricated field-emitter arrays are presently being investigated for use in such technologically important applications as microwave amplifiers and flat-panel displays.[1] To facilitate their incorporation into various devices, we are investigating processing procedures through which the performance of field-emitter arrays can be enhanced.

This performance enhancement is a multifaceted goal involving such aspects as operational voltage reduction, the rapid achievement of emission current stability at relatively high current-per-tip loading levels ($I > 10\ \mu A$/tip), and increasing emission current uniformity from each tip and between tips in the array. To quantify the basic principles involved in array performance enhancement, we recall the Fowler-Nordheim equation,[2,3] which describes the current-voltage (I-V) characteristic of the electron field-emission process,

$$I/V^2 = \alpha a\, \beta^2 \exp(-b\phi^{3/2}/\beta V).$$

Here, I is the electron current, V the applied voltage, a and b are essentially constants, α is the emitting area, ϕ is the average work function of the emitter surface, and β is the proportionality factor between the applied voltage and the electric field, E, at the emitting surface, $E = \beta V$.

It is clear that to enhance emitter array performance one must control ϕ and β; that is ϕ and β should optimally be identical from tip to tip in the array. This amounts to controlling the chemical state and physical structure of the emitter array surfaces. Therefore, any post array fabrication processing procedures developed to enhance performance are best performed *in situ* prior to, or following, tube seal-off.

The first step towards control of the emitter surface chemistry is to "clean" the emitter array surfaces. During their fabrication and handling, exposure to the ambient atmosphere will lead to carbonaceous surface contamination and in many cases oxidation.[4] Previous investigations have shown that *in situ* hydrogen plasma treatment to ion doses of 10^{18} to 10^{19} ions/cm^2 results in a work function decrease of ~ 1 eV and improvements in the emission uniformity in the case of both microfabricated single tips and arrays.[5] This is presumably due to the removal of the surface contaminants. The cleaning action of the hydrogen reaches completion as there exists a dose in the range of 10^{18} to 10^{19} ions/cm^2 beyond which no further changes in the I-V characteristics are observed. Lastly, preliminary investigations have shown that contaminant removal via hydrogen plasma treatment allows for *immediate* turn-on of the array to relatively high current-per-tip loading levels (≥ 5 μA/tip) without disruptive vacuum arcs that lead to emitter tip array destruction. In the past, array destruction could occur frequently if relatively long emitter seasoning procedures were not employed wherein gradual increases in emission current were made until the final operating level was reached; seasoning time periods could be on the order of 50 to 100 hours.

Given the apparent surface cleanliness achieved with hydrogen glow discharge processing we turn to the question of further enhancing emission uniformity across emitter arrays; this to a large degree focuses on the detailed geometrical structure of the emitter tips at their apices.

Control of the geometrical structure of the emitter array surfaces can be considered on two approximate length scales L_1 and L_2, where $L_1 \geq 100$ Å and $L_2 < 100$ Å. The L_1 range is fairly well controlled in modern microfabrication processes; in the case of emitter arrays this refers to the general tip shape, gate hole diameters, tip-to-gate spacing, and so forth. In the range of L_2, however, many factors emerge, particularly involving details of the emitter tip shape, which are difficult to control and have a profound effect on β. For example, in the case of polycrystalline emitter tips grain size, shape, and orientation are important. In addition, for all

types of emitter tips the presence of clusters of surface atoms and the resulting field-enhancing effects should be expected. For reference we recall that a conducting hemisphere on a conducting flat plane produces a field enhancement factor of 3 at its apex over that of the field on the plane far removed from the hemisphere.[6] As the emission current is exponentially dependent on β, the details of the emitter tip shape at length scales of < 100 Å are very important and some degree of control over these physical aspects is required if emission uniformity across the array is to be achieved.

In the research presented here we have studied the effects of combining hydrogen plasma treatment with glow discharges involving inert gases to investigate the effect on ϕ and β of supplementing the chemical cleaning action of the hydrogen with the sputtering action of relatively low energy inert gas ions. Relatively high energy inert gas ion bombardment (> 1 keV) is commonly employed for the sputter cleaning of surfaces[4] and the sharpening of conventional field-emitter tips.[7]

II. EXPERIMENTAL

The experimental chamber is an ultra-high vacuum (UHV) field-emission microscope constructed of metal and glass with a base pressure of $< 3 \times 10^{-11}$ torr following a 12-hour bakeout at 250 °C. All experiments were conducted at room temperature.

Array performance data is collected in the form of I-V characteristics and by direct viewing of the electron-emission spatial distribution on a phosphor screen.

The microfabricated emitter tips were of the type developed at SRI: metal-insulator-metal, employing SiO_2 as the insulating layer between a molybdenum gate and molybdenum emitter tips, as shown in Figure 1.

Glow discharges were operated with a current-regulated direct current supply. During glow discharge processing the base and gate of the emitter array were electrically connected and served as the cathode in the discharge; thus, the array structure was bombarded only by ions. The anode of the glow discharge was ~1 cm from the cathode. At this distance, pressures of ~1 torr and operating voltages of ~275 to 450 V were required to sustain a glow discharge in the gases employed. Total ion current densities at the emitter array were on the order of 1×10^{16} ions/cm^2/s. Gases used were research-grade purity (99.9999%) and admitted to the system from 1-*l* glass flasks. Following glow discharge treatment the system was evacuated to UHV conditions prior to array operation.

III. RESULTS

To determine the effects of inert gas ion bombardment on emitter array performance, the arrays were first cleaned by hydrogen plasma treatment. This procedure was used to produce chemically similar surfaces with which the changes produced by subsequent bombardment with various inert gas ions could be investigated.

A. Hydrogen and neon glow discharges

Following installation of the emitter array in the microscope and system bakeout, I-V characteristics were collected from the emitter array. An example of such data, for a 127-tip array, is shown in Figure 2 (curve A) as a Fowler-Nordheim (FN) plot.

Next, the array was treated in a hydrogen glow discharge under the conditions described above to a dose of 10^{18} ions/cm^2. The initial results of hydrogen glow discharge cleaning of emitter arrays have been reported.[5] After evacuating the system to UHV conditions the I-V data shown in curve B of Figure 2 were accumulated. Note the reduction in voltage required to

achieve a given current relative to the I-V characteristics shown in curve A. The field-emission micrographs corresponding to the FN data in Figure 2, curves A and B, are shown in Figures 3a and 3b, respectively. Note in the patterns that although the change in the emitting area appears to be rather small there is an increase in the emission uniformity. This was typically observed with all emitter arrays studied.

To investigate the effects of mild sputtering on array performance, hydrogen cleaning was followed by neon bombardment. The results of glow discharge processing using He + 10% Ne and H_2 + 10% Ne to equivalent ion doses were similar. Curve C, Figure 2, shows the I-V characteristics of the 127-tip array following treatment in H_2 + 10% Ne to a total ion dose of 2×10^{19} ions/cm^2 (~2×10^{18} ions/cm^2 of Ne^+). In general, the slope following H_2 + 10% Ne treatment varied from being slightly less than to slightly greater than (but within ~10% of) the slope of the post-H_2 treated array. However, a sufficient ion dose could be achieved after which: (1) the slope of the post-H_2/Ne-plasma-treated array FN data was approximately equal to or greater than for the hydrogen-plasma-treated array (curve B), and (2) a decrease in emission current at a given voltage relative to curve B occurred.

The effect of this treatment as observed in the electron-emission pattern, shown in Figure 3c, is very interesting. We note that our 127-tip arrays are fabricated such that the border of the array is a hexagon. This hexagonal shape is evident in the emission pattern of Figure 3c; for reference, the orientation of the hexagon is shown in the upper right corner of the figure. The appearance of the array shape in the emission pattern following Ne/H_2 plasma treatment was often observed with the 127-tip arrays and the 100-tip arrays (square pattern due to the 10×10 packing arrangement) that we have investigated. These observations indicate that such treatment significantly enhances emission uniformity across the arrays; we estimate that *at least* 50% of the tips in the array must be participating in the emission process for such a definition of the array shape to result.

Ne/H_2 treatment induces changes in the I-V characteristics and emission pattern up to Ne^+ doses of typically ~ 10^{18} ions/cm^2; thereafter, changes are much slower following an equivalent dose.

Similar experiments have also been conducted employing single microfabricated field-emitter tips. In general, the changes in the I-V characteristics of the single emitter tips were similar to those observed with the arrays. However, in particular cases the emission current at a given voltage could be increased at some point with H_2/Ne bombardment as is discussed below.

The FN data are shown in Figure 4 for a single tip. Curve A is the data following installation in the system and bakeout. After hydrogen plasma treatment to a dose of 10^{18} ions/cm^2, the data in curve B were collected. Again, note the reduction in the voltage required for a given current when compared with curve A. The field-emission patterns corresponding to the pre- and post-hydrogen-plasma-treated tip are shown in Figures 5a and 5b, respectively. A slight increase in the emitting area is observed and a distinct improvement in the emission uniformity has occurred. This was a general trend observed with single emitter tips. Note that in the case shown here, hydrogen plasma treatment resulted in the disappearance of a spurious emission site in the lower right corner of the pattern in Figure 5a. This indicates that the large emitting area shown in Figures 5a and 5b is a region that protrudes from the emitter tip apex.

Following the hydrogen plasma treatment the emitter was exposed to the H_2 + 10% Ne plasma. Curve C shows the I-V characteristics after a dose of ~1×10^{17} ions/cm^2 of Ne, and curve D after ~ 7×10^{17} ions/cm^2 Ne. Note that in curve C the current for a given voltage has increased relative to curve B. However, following a sufficient Ne dose the emission current for a given voltage decreases relative to curve B, as shown in curve D. The field-emission pattern corresponding to curve D is shown in Figure 5c. A significant increase in emitting area and emission uniformity is evident in the micrograph.

B. Hydrogen and xenon glow discharges

The experiments involving Xe and H_2 were conducted in the same manner as those involving Ne and H_2. Again, the results for arrays and single emitter tips were similar.

Following installation of a single tip and system bakeout, the I-V characteristics shown in curve A, Figure 6, were collected. Hydrogen plasma treatment to a dose of ~ 1×10^{18} ions/cm^2 resulted in the subsequent I-V characteristic shown in curve B of Figure 6. The corresponding field-emission patterns for the pre- and post-hydrogen-plasma-treated emitter are shown in Figures 7a and 7b, respectively. Note again that the decrease in voltage for a given current is accompanied by an increase in the emission uniformity from the emitter tip.

Plasma treatments involving H_2 + 10% Xe were subsequently performed. Curve C in Figure 6 shows the I-V characteristics obtained after a dose of 5×10^{16} ions/cm^2. Figure 7c is a field-emission micrograph of the emitter taken following the I-V characteristics of curve C, Figure 6. H_2/Xe treatment often resulted in the currents for a given voltage exceeding those required prior to hydrogen plasma treatment for single emitter tips and arrays. Following a subsequent dose of ~ 5×10^{17} ions/cm^2 the emitter tip was shorted (gate to base). As opposed to Ne (and He) treatments, the occurrence of emitter destruction and/or the presence of gate to base leakage was higher when arrays and single tips were exposed to the H_2/Xe discharge, even at a lower total ion dose.

C. Hydrogen and helium glow discharges

The effects of helium ion bombardment on emitter array characteristics were also investigated under conditions similar to those utilized for neon and xenon. With mixtures of H_2 + 10 % He, applied potentials of ~300 V, and doses of ~10^{18} ions/cm^2, only small changes in the I-V characteristics of the post-hydrogen-plasma-treated arrays and single tips were observed. Voltages for a given current increased by a few percent and small increases in slope (<10 %)

occurred. In addition, only slight changes in the emission patterns were observed with a barely perceptible increase in emission uniformity.

IV. DISCUSSION

To analyze our results, we begin by estimating the ion energies at the cathode (array) under our glow discharge conditions. The ion energies in a relatively high pressure glow discharge, as is the case here, are distributed from near zero to the full anode-to-cathode potential, V_0, making detailed characterization difficult. A reasonable estimate of the "average" ion energy can be found if we calculate the energy of ion type x, E_x, gathered in a mean free path, λ, in the cathode dark space.[8,9]

$$E_x = [\sqrt{2}\,\lambda_x]\, V_{0x} / d_x$$

where d_x is the thickness of the dark space for the discharge involving ion x. We assume that the entire applied voltage appears across the cathode dark space, thereby maximizing the energy. The $\sqrt{2}$ term corrects for the ionic as opposed to the neutral molecular mean free path.[10]

With d ~ 0.1 cm in all cases, the applied potentials and calculated ion energies are shown in Table 1. The λ's shown in the table are calculated for the gas mixtures shown and apply to the inert gas ion component.[10] We see that these ion energies are well below the sputtering threshold energies of molybdenum—that is, the majority of ions do not sputter the emitter tips. To obtain an absolute maximum on the sputtering yield, Y_{max}, we can take the ion energy to be the full anode-to-cathode potential V_0. This upper limit to the sputtering yield can be found from a combination of experimental data and empirical formulae[11,12]; these yields, for an ion dose, D, are also shown in Table 1. It should be noted that significant errors in the sputtering yield can result from relatively small errors in the ion energy calculation as the sputtering yields are not

well known and in addition are a sensitive function of energy for energies of ~ 100 eV, particularly in the cases of Ne and Xe.[12]

A. Hydrogen

In the case of the pure hydrogen plasma, as has been discussed,[5] it is reasonable to assume that a work function change due to contaminant removal accounts for the shift in the I-V characteristics as the sputtering of molybdenum by hydrogen at the energies and doses investigated here is totally negligible; even at doses of 10^{19} ions/cm^2 H_2^+ with the full cathode-to-anode potential energy of 300 V and neglecting the dissociation of the molecular ion upon impact, only ~10^{-1} monolayers of molybdenum would be removed. The work function change can be extracted from the slope of the FN curves shown in Figure 2.[3,5] If we assume that the average work function of the emitters following hydrogen plasma treatment is that of hydrogen-covered molybdenum, 4.9 eV, we find that hydrogen plasma treatment reduced the effective work function of the array (Figures 2 and 3) by 1.5 eV, and the single tips by 1.4 eV (Figures 4 and 5) and 0.5 eV (Figures 6 and 7). Typical work function changes are 1 eV for hydrogen ion doses of 10^{18} to 10^{19} ions/cm^2; however, changes ranging from 0.5 - 1.5 eV with single tips and arrays have been observed.[5] The resulting slight increases in emitting area and uniformity of the arrays following hydrogen treatment are due to the participation of more tips in the emission process and an improvement in the uniformity of emission from those tips participating.[5]

B. Helium

In helium bombardment, the average ion energies calculated are again near or below the threshold energy for sputtering of the molybdenum tips. The upper limit to the yield, as shown in Table 1, is ~ 2 monolayers of molybdenum for the doses investigated here. The slight changes in the I-V characteristics and emission patterns observed are most likely due primarily to atom displacements by ion-bombardment-activated surface diffusion. This hypothesis is consistent with the fact that the slight changes in the I-V characteristics rapidly saturate; that is for doses of

~ 10^{16} ions/cm^2 to ~ 10^{17} ions/cm^2 of helium no significant changes in the I-V characteristics occur, and only slight variations in the details of the emission pattern are observed.

C. Neon and xenon

The situation in which surface sputtering is nonnegligible is rather complicated to explain unequivocally. It is clear from the emission patterns of single tips and arrays that the emission area and uniformity are significantly increased following H_2/Ne and H_2/Xe plasma treatment. Such an improvement has not been observed with H_2 treatment alone. Unfortunately, the physical details leading to the changes observed in I-V characteristics are difficult to extract from the FN data. We have, of course, three variables—the area α (proportional to the intercept of the FN plots), ϕ, and β. Although ideally emitting areas can be found directly from the FN data without a detailed knowledge of ϕ or β, the presence of surface adsorbates can severely skew these calculations. In our case, large amounts of chemisorbed hydrogen are most likely present on the emitter surfaces. As hydrogen is known to decrease the microscopic emitting area of tungsten emitters[13] by a factor of ~10, we would expect to see such a result with molybdenum as the two are chemically similar. This unknown variation in α, in addition to the fact that the FN intercept depends on ϕ and β, makes changes in the FN intercepts difficult to interpret. A qualitative explanation of the changes in the slope of the FN plots induced by inert gas ion bombardment is possible, however.

Inert gas ion bombardment is observed to lead to an increase in slope of the FN plots. We recall that the slope of the FN plot, S_{FN}, varies as

$$S_{FN} \propto \phi^{3/2}/\beta.$$

During the initial stages of inert gas ion bombardment, we might expect to see changes in both ϕ and β. Some initial atomic-scale surface roughening should occur, and can be accounted for by an effective *decrease* in the average surface work function. This follows from the fact that low-index (atomically smooth) crystal planes have a higher work function than high-index

(atomically rough) crystal planes.[14] The average surface work function may also be decreased by the sputtering of contaminants not removed by the hydrogen plasma treatment. Both of these factors in themselves would lead to a decrease in the slope of the FN plot, a trend that is not observed. Thus, we conclude that decreases in β dominate the change (increase) in slope observed following bombardment. The changes in the I-V characteristics observed with Ne and Xe are generally consistent with this hypothesis. The sputtering and ion-bombardment-activated surface diffusion apparently lead to a net smoothing of the emitter surface and therefore a decrease in β. Note that as protuberances present a greater surface-area-to-volume ratio than does the bulk structure of the emitter tip, their preferential sputtering and/or dispersion would be expected. The subsequent increase in emission uniformity is due to the variation in sputtering rate with the emitter tips' β. The β of 'blunt' tips changes more slowly because of sputtering than does the β of relatively 'sharp' emitter tips—that is, more material must be removed from a large tip, relative to that required for a smaller tip, to achieve an equivalent change in β. Thus, the emitter tips tend to approach an equilibrium shape, thereby leading to an enhancement in emission uniformity across the array.

Because of the large ion energy spread in the glow discharge, it is difficult to quantify the quantity of emitter tip material sputtered during our investigations. From our ion energy calculations we can conclude only that for inert gas ion doses of 10^{18} ions/cm^2, much less than ~ 30 and 70 monolayers of molybdenum are removed by Ne^+ and Xe^+, respectively. Although the calculations indicate that the absolute yield of molybdenum for a given ion dose is of the same order for Ne^+ and Xe^+, we observe relatively dramatic changes in the I-V characteristics for Xe^+ doses only on the order of 10^{16} to 10^{17} ions/cm^2. In addition, the use of Xe, despite the improvement in uniformity observed, often leads to leakage (base to gate) and/or apparent vacuum-arc-intitiated emitter tip destruction. Neon bombardment reproducibly leads to significant improvements in emission uniformity without causing leakage and arcing as is often the case with Xe. At this point, we have been unable to reconcile this discrepancy. If it were

possible to calculate or measure the ion energy distributions, and thereby determine accurate sputtering yields for Ne and Xe, we could address this observation in more detail.

The improvement in emission uniformity from individual tips and between tips in an array as a result of Ne and Xe cathode bombardment is evident in these investigations. The net apparent smoothing effect due to the removal of protuberances by inert gas ion bombardment that we have observed in our experiments is undoubtedly related to the phenomenon of electrode "conditioning" of high-voltage gaps. In this process the voltage hold-off capability can be increased following low-energy ion bombardment from glow discharges.[15] This increase in breakdown strength is most likely due, at least in part, to the removal of field-enhancing protuberances on the electrode surfaces, leading to locally enhanced field-electron emission (from the cathode) and eventually a vacuum arc.

V. CONCLUSIONS

Hydrogen plasma treatment in conjunction with neon and xenon ion bombardment leads to a significant enhancement in the electron-emission uniformity for each tip and between tips in the array. The effect of the ion bombardment is a net smoothing of the emitter tip surfaces by low-energy sputtering. The process tends to bring the emitter tips to a similar shape by mild sputtering, as tips having greater field enhancement factors are blunted faster than those having a lower enhancement factor, thereby allowing an equilibrium size/shape to be approached. Under our experimental conditions the best results were obtained with Ne. Helium has little effect on the uniformity and with Xe bombardment, leakage and emitter tip destruction are prevalent .

These processes can be readily implemented in technological tube applications as they may be performed *in situ* prior to tube seal-off.

ACKNOWLEDGMENTS

The authors acknowledge helpful discussions with I. Brodie and C.E. Holland during the course of this work. In addition, we thank B.V. Conroy of SRI's glassblowing shop for his assistance in equipment construction and the members of the Vacuum Microelectronics Group—D.A. Thibert, S. Chhokar, S. Shepherd, and L. Wachsman—for emitter tip fabrication. This work was supported by the Advanced Research Projects Agency under Contract No. MDA972-91-C-0029.

REFERENCES

[1]I. Brodie and C.A. Spindt, in *Advances in Electronics and Electron Physics*, edited by P.W. Hawkes (Academic Press, New York, 1992), Vol. 83, Chap. 1, pp. 2–95.

[2]R.H. Fowler and L.W. Nordheim, Proc. Roy. Soc. (London) A **119**, 173 (1928).

[3]R. Gomer, *Field Emission and Field Ionization* (Harvard University Press, Cambridge, MA, 1961).

[4]G.A. Somorjai, *Chemisry in Two Dimensions: Surfaces* (Cornell University Press, Ithaca, NY, 1981).

[5]P.R. Schwoebel and C.A. Spindt, Appl. Phys. Lett. **63**, 33 (1993).

[6]J.A. Stratton, *Electromagnetic Theory* (McGraw-Hill, New York, 1941).

[7]M.K. Miller and G.D.W. Smith, *Atom Probe Microanalysis: Principles and Applications to Materials Problems* (Materials Research Society, Pittsburgh, PA, 1989).

[8]A. von Engel, *Ionized Gases* (Oxford University Press, London, 1955).

[9]L.B. Loeb, *Fundamental Processes of Electrical Discharge in Gases* (Wiley, New York, 1939).

[10]S. Dushman, *Scientific Foundations of Vacuum Technique* (Wiley, New York, 1962).

[11]M. Kaminsky, *Atomic and Ionic Impact Phenomena on Metal Surfaces* (Academic Press, New York, 1965).

[12]H.H. Andersen and H.L. Bay in *Sputtering by Particle Bombardment I*, edited by R. Behrisch (Springer, New York, 1981).

[13]R. Gomer, R. Wortman, and R. Lundy, J. Chem. Phys. **26**, 1147 (1956).

[14]R. Smoluchowski, Phys. Rev. **60**, 661 (1941).

[15]R.V. Latham, *High Voltage Vacuum Insulation: The Physical Basis* (Academic Press, New York, 1981).

TABLES

Table 1

Gas	V_0 (volts)	λ (cm)	$E_{Average}$ (eV)	D_{Total} (ions/cm^2)	Y_{max} (atoms/cm^2)	$E_{threshold}$ (eV)
H_2	275	9.3×10^{-3}	H_2^+ 36	10^{18}	1×10^{13}	~75
H_2 + 10% He	300	6.0×10^{-3}	He^+ 25	10^{18}	2×10^{15}	~48
H_2 + 10% Ne	300	3.0×10^{-3}	Ne^+ 13	10^{18}	3×10^{16}	~30
H_2 + 10% Xe	450	8.0×10^{-4}	Xe^+ 25	10^{18}	7×10^{16}	~48

FIGURE CAPTIONS

FIG. 1. A schematic of the field-emitter array. The base is single-crystal silicon and the field-emitter cathodes and gate film are vapor-deposited molybdenum. The insulating layer is thermally grown SiO_2.

FIG. 2. Fowler-Nordheim data showing the effect of pure hydrogen and hydrogen + 10% neon plasma treatment on a 127-tip field-emitter array. Line A: FN data prior to hydrogen plasma treatment. Line B: FN data following hydrogen plasma treatment (dose $\sim 1 \times 10^{18}$ ions/cm^2). Line C: FN data following hydrogen + 10% neon plasma treatment (total dose $\sim 2 \times 10^{19}$ ions/cm^2).

FIG. 3. Field electron micrographs corresponding to the FN data shown in Figure 2. (a) Electron micrograph of the 127-tip array prior to hydrogen plasma treatment (V = 147 V, I = 1 μA). (b) Electron micrograph of the array following hydrogen plasma treatment (V = 107 V, I = 1 μA). (c) Electron micrograph of the array following hydrogen + 10% neon plasma treatment (V = 120 V, I = 1 μA).

FIG. 4. Fowler-Nordheim data showing the effect of pure hydrogen and hydrogen + 10% neon plasma treatment on a microfabricated single-tip field emitter. Line A: FN data prior to hydrogen plasma treatment. Line B: FN data following hydrogen plasma treatment (dose $\sim 1 \times 10^{18}$ ions/cm^2). Line C: FN data following hydrogen + 10% neon plasma treatment (total dose $\sim 1 \times 10^{18}$ ions/cm^2). Line D: FN data following an additional hydrogen + 10 % neon dose of 7×10^{18} ions/cm^2.

FIG. 5. Field electron micrographs corresponding to the FN data shown in Figure 4. (a) Electron micrograph, corresponding to curve A in Figure 4, of the single tip prior to

hydrogen plasma treatment (V = 175 V, I = 1 μA). (b) Electron micrograph of the tip following hydrogen plasma treatment, curve B, Figure 4 (V = 133 V, I = 1 μA). (c) Electron micrograph of the single tip following hydrogen + 10% neon plasma treatment, curve D, Figure 4 (V = 130 V, I = 1 μA).

FIG. 6. Fowler-Nordheim data showing the effect of pure hydrogen and hydrogen + 10% xenon plasma treatment on a microfabricated single-tip field emitter. Line A: FN data prior to hydrogen plasma treatment. Line B: FN data following hydrogen plasma treatment (dose ~ 1×10^{18} ions/cm^2). Line C: FN data following hydrogen + 10% xenon plasma treatment (total dose ~ 5×10^{16} ions/cm^2)..

FIG. 7. Field electron micrographs corresponding to the FN data shown in Figure 6. (a) Electron micrograph of the single tip prior to hydrogen plasma treatment (V = 116 V, I = 0.2 μA). (b) Electron micrograph of the tip following hydrogen plasma treatment (V = 192 V, I = 0.2 μA). (c) Electron micrograph of the single tip following hydrogen + 10% xenon plasma treatment (V = 128 V, I = 0.2 μA).

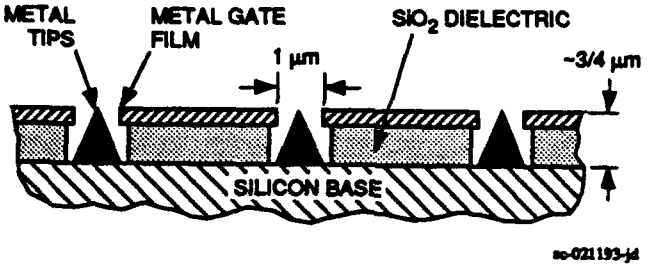
METAL TIPS
METAL GATE FILM
1 μm
SiO_2 DIELECTRIC
~3/4 μm
SILICON BASE
ao-021193-jd

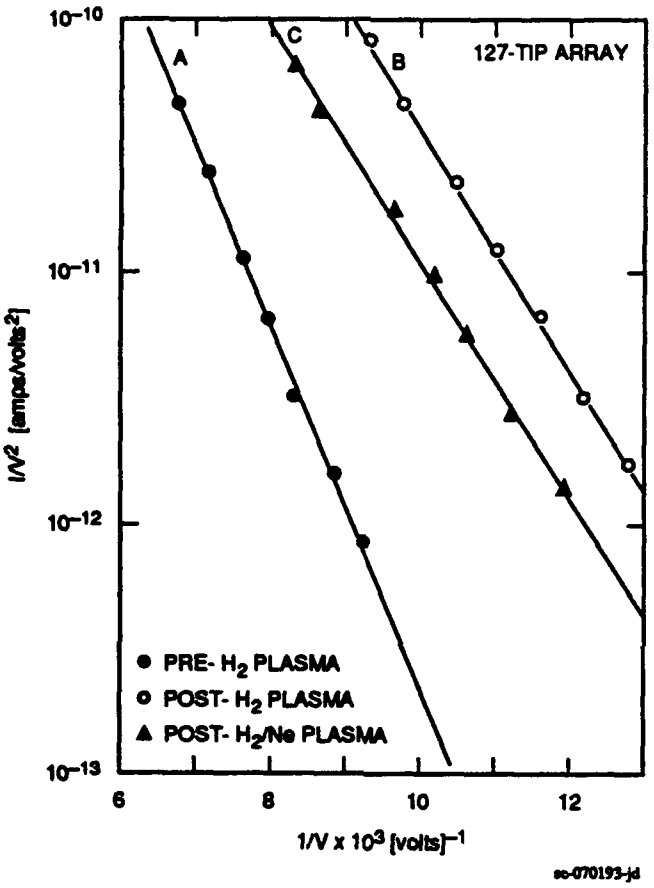
127-TIP ARRAY
A
B
C
10^{-10}
10^{-11}
10^{-12}
10^{-13}
I/V^2 [amps/volts^2]
6
8
10
12
$1/V \times 10^3$ [volts]$^{-1}$
● PRE- H_2 PLASMA
○ POST- H_2 PLASMA
▲ POST- H_2/Ne PLASMA
sc-070193-jd

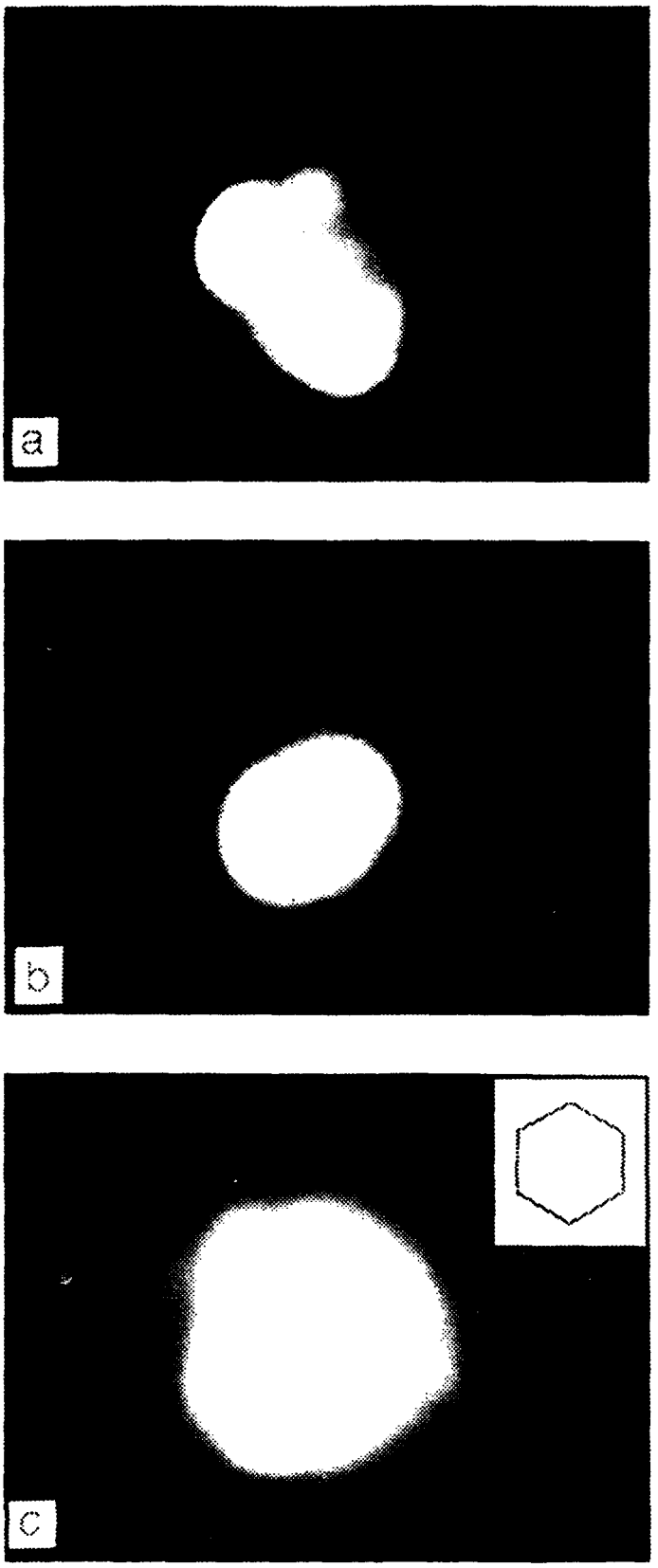

sp-6520[illegible]

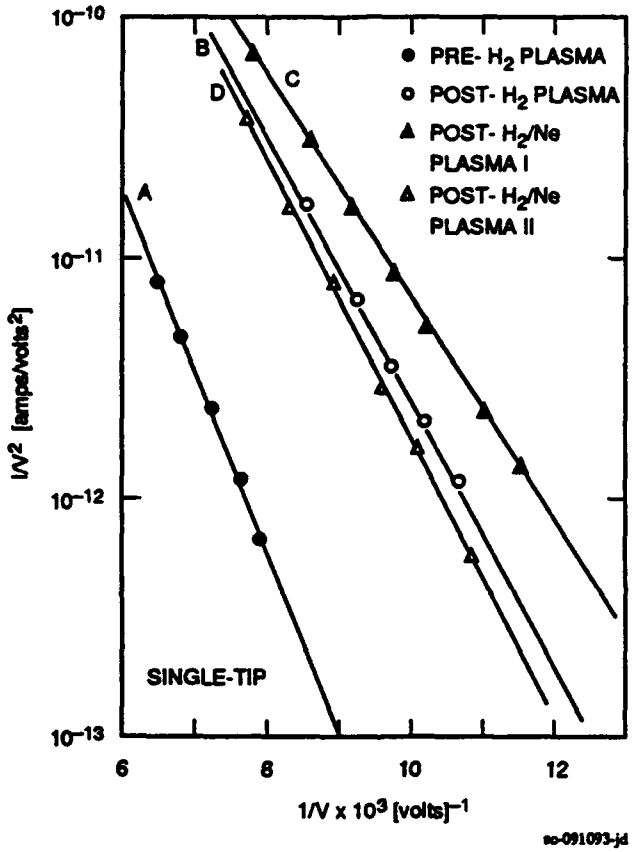
10^{-10}
10^{-11}
10^{-12}
10^{-13}
I/V^2 [amps/volts^2]
A
B
C
D
● PRE- H_2 PLASMA
○ POST- H_2 PLASMA
▲ POST- H_2/Ne PLASMA I
▲ POST- H_2/Ne PLASMA II
SINGLE-TIP
6
8
10
12
1/V x 10^3 [volts]$^{-1}$
so-091093-jd

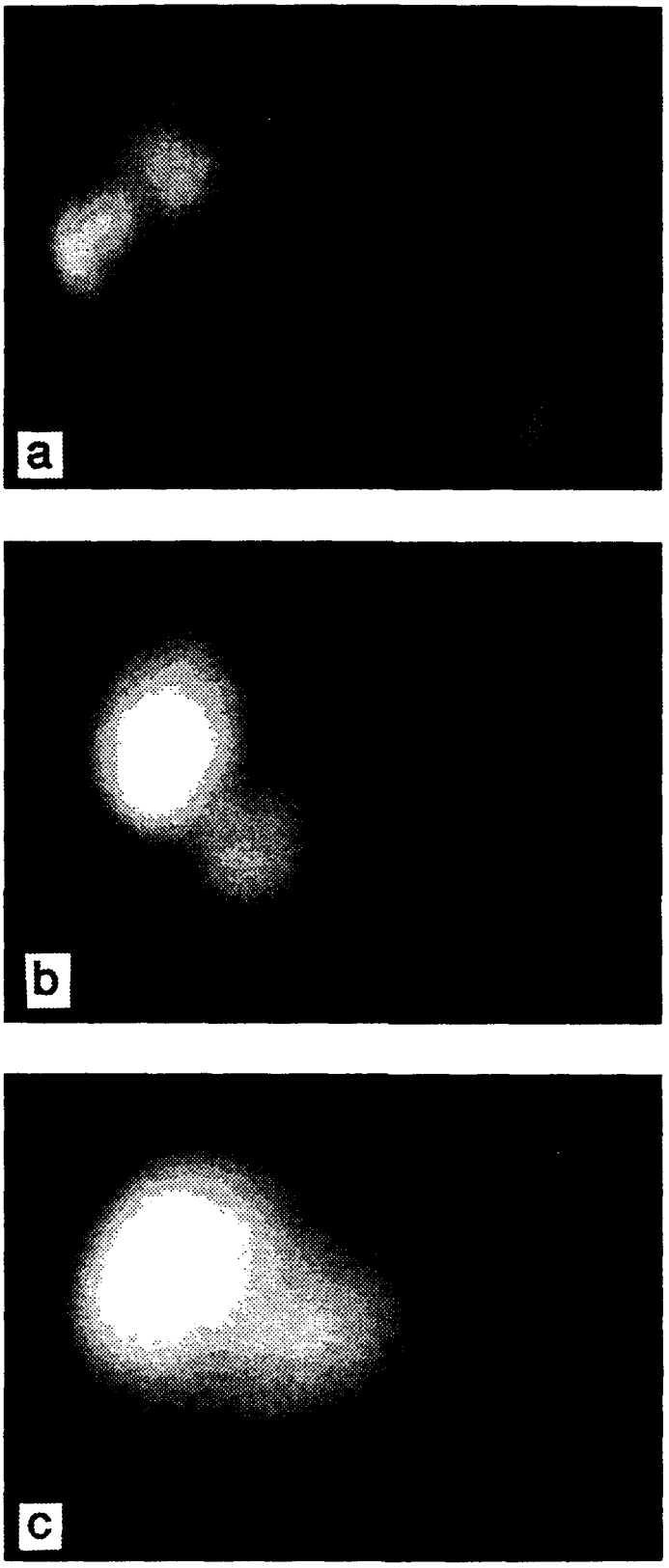

sp-752094-sd

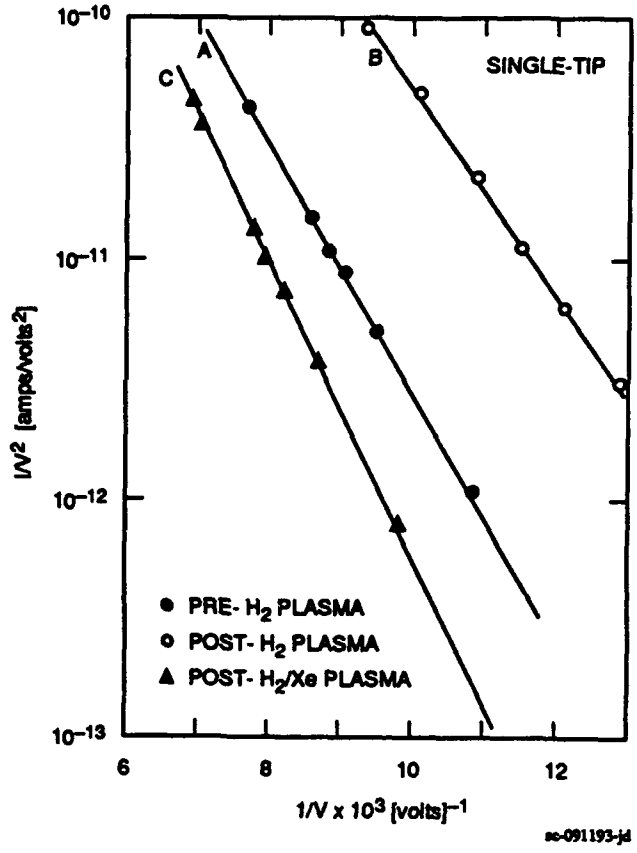
SINGLE-TIP
A
B
C
PRE- H_2 PLASMA
POST- H_2 PLASMA
POST- H_2/Xe PLASMA
10^{-10}
10^{-11}
10^{-12}
10^{-13}
I/V^2 [amps/volts^2]
6
8
10
12
$1/V \times 10^3$ [volts]$^{-1}$
ac-091193-jd

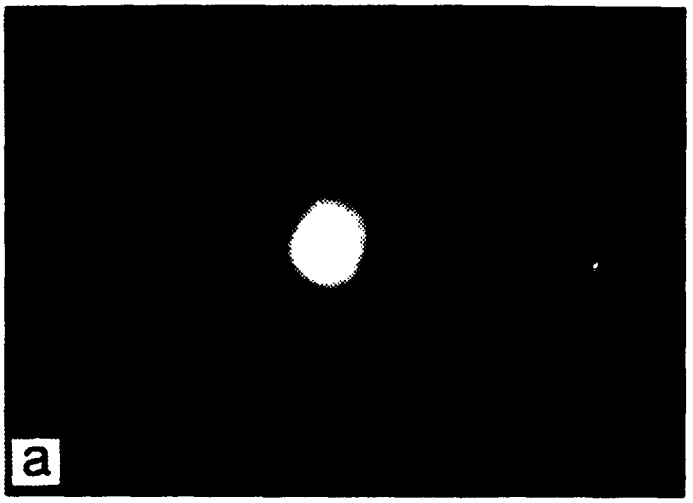

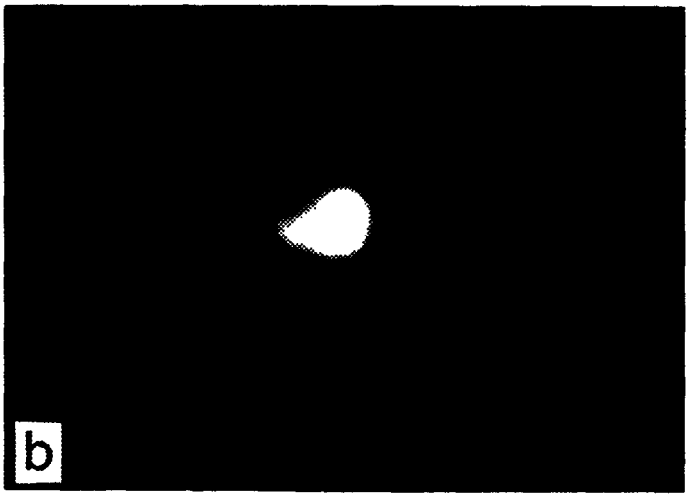

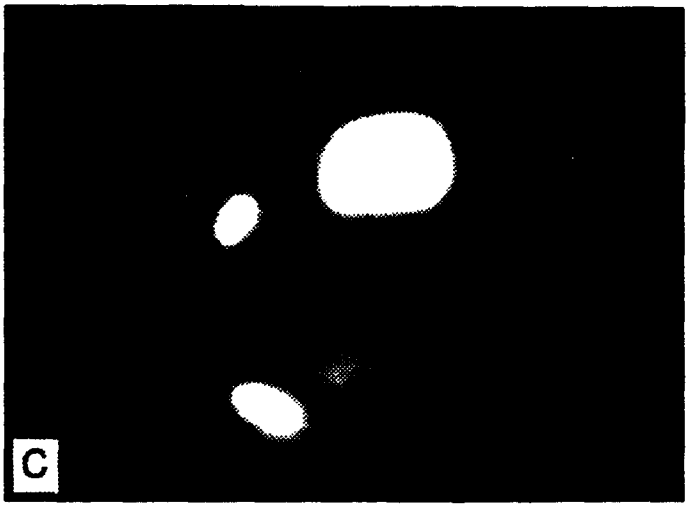

sp-852094-sd